Quantum sensing in an exciton-polariton condensate

Jorge Chávez-Carlos,[1] Daniela Garrido-Ramírez,[2] A. J. Vega Carmona,[3] Victor S. Batista,[4] Francisco Pérez-Bernal,[5,6] Carlos A. Trallero-Herrero,[1] M. A. Bastarrachea-Magnani,[3] and Lea F. Santos[1]

[1] *Department of Physics, University of Connecticut, Storrs, Connecticut 06269, USA*
[2] *Faculty of Sciences, University National Autonomus of Mexico,. Postal 70-543, C.P. 04510, Cd. Mx, Mexico*
[3] *Departamento de Física, Universidad Autónoma Metropolitana-Iztapalapa, Av. Ferrocarril San Rafael Atlixco 186, C.P. 09310 CDMX, Mexico.*
[4] *Department of Chemistry, Yale University, P.O. Box 208107, New Haven, Connecticut 06520-8107, USA*
[5] *Departamento de Ciencias Integradas y Centro de Estudios Avanzados en Física, Matemáticas y Computación, Universidad de Huelva, Huelva 21071, Spain*
[6] *Instituto Carlos I de Física Teórica y Computacional, Universidad de Granada, Granada 18071, SPAIN*

The extreme sensitivity of critical systems has been explored to improve quantum sensing and weak signal detection. The closing of the energy gap and abrupt change in the nature of the ground state at a quantum phase transition (QPT) critical point enhance indicators of parameter estimation, such as the quantum Fischer information. Here, we show that even if the system lacks a QPT, the quantum Fischer information can still be amplified due to the presence of an excited-state quantum phase transition (ESQPT). This is shown for a light-driven anharmonic quantum oscillator model that describes the low-lying spectrum of an exciton-polariton condensate proposed as a platform for quantum computation. In the classical limit, the ESQPT translates into the emergence of a hyperbolic point that explains the clustering of the energy levels at the vicinity of the ESQPT and the changed structure of the corresponding eigenstates, justifying the enhanced sensitivity of the system. Our study showcases the relationship between non-conventional quantum critical phenomena and quantum sensing with potential experimental applications in exciton-polariton systems.

Quantum metrology and quantum sensing aim to use quantum properties to enhance measurement precision beyond what could be classically achieved [1, 2]. Entanglement, for example, is a pure quantum property that has been used to improve measurement sensitivity [3–7], but several other mechanisms have been explored [2]. Squeezed light has been used to improve the sensitivity of detectors based on laser interferometry [8, 9]. Another promising avenue is quantum criticality, which extends the use of phase transitions in classical sensing to the quantum domain. The diverging susceptibility of the ground state at a quantum phase transition (QPT) can, in principle, be used to enhance parameter estimation and to saturate the Heisenberg limit [10–22]. Experimentally, access to external control parameters that allow reaching critical points are of extreme importance to tune a sensing platform. Here, we present a system that can be taken into a critical state through simple light control.

The abrupt change in the nature of a quantum state $|\Psi_j\rangle$ that takes place as a (set of) control parameter(s) λ of a system reaches the critical point of a QPT is reflected in the increasing value of the quantum Fisher information (QFI) defined as [23, 24],

$$F_\lambda^{(j)} = 4\sum_{i\neq j} \frac{|\langle\Psi_i|\partial_\lambda \hat{H}|\Psi_j\rangle|^2}{(E_i - E_j)^2}, \tag{1}$$

where $\partial_\lambda := \frac{\partial}{\partial\lambda}$, $\hat{H}(\lambda) = \hat{H}_0 + \lambda\hat{H}_1$ is the Hamiltonian that describes the system, E_i are its eigenvalues, and $|\Psi_i\rangle$ its eigenstates. Usually, $F_\lambda^{(j)}$ is computed for the ground state ($j = 0$), but the analysis can be extended to other states. $F_\lambda^{(j)}$ is equivalent to the quantum fidelity susceptibility [25], which is the second-order term in the Taylor expansion of the fidelity $|\langle\Psi_j(\lambda)|\Psi_j(\lambda+\delta\lambda)\rangle|$ between two states $|\Psi_j\rangle$ obtained for two values of the control parameter that differ by an infinitesimal amount $\delta\lambda$. The QFI also coincides with the real part of the quantum geometric tensor [15, 26], which measures the distance between two states. The importance of the QFI for quantum sensing becomes evident with the quantum Cramér–Rao bound, which states that the inverse of $F_\lambda^{(0)}$ limits the accuracy of an unbiased estimation of a system parameter [23, 24]. At a QPT, in particular, where the energy gap between the ground-state E_0 and the first-excited state energies vanishes, the QFI peaks, indicating improved sensitivity and enhanced measurement precision.

The merging of energy levels is not restricted to the two lowest levels. It can propagate to higher excitation energies as the control parameter increases beyond the ground-state critical point, a phenomenon that became known as excited state quantum phase transition (ESQPT) [27]. Despite the increasing interest in ESQPTs [28] and its consequences to localization [29, 30], the subject has not yet received much attention in the context of quantum metrology. There are systems that present both a QPT and an ESQPT, but only their QPT was explored for quantum sensing, such as the Lipkin–Meshkov–Glick model [16, 31] and the Kerr parametric oscillator [21, 32]. The latter, in particular, can be realized in superconducting circuits, where the energy levels can be experimentally measured as a function of

the control parameter [33], thus allowing for the detection of the ESQPT [34]

Here, we investigate an anharmonic quantum oscillator model that describes the low-lying spectrum of an exciton-polariton condensate whose polariton interactions lead to a Kerr-like nonlinearity [35]. Remarkably, the system exhibits an ESQPT without a QPT. It can be taken to the ESQPT critical point by light control, where we find an enhancement of the QFI. This happens not only for the excited states in the vicinity of the ESQPT critical energy, but for the states all the way down to the ground state. This analysis sheds light on the interplay between the structures of quantum states and critical phenomena, with consequences that could be experimentally detected and built up for sensing devices in exciton-polariton condensates.

Exciton-polariton condensate model.— We consider an exciton-polariton condensate at zero momentum formed inside a semiconductor microcavity pumped with an external coherent optical field [35–38]. Exciton-polaritons offer a promising platform for tunable Kerr-like nonlinearities [39]. These quasiparticles emerge when photons get dressed by the excitons in the semiconductor under a strong light-matter coupling regime [40]. By inheriting the properties of their original constituents, polaritons yield effective photon interactions [41], that allow for the creation of macroscopic quantum phenomena with novel features due to their non-equilibrium character [41, 42], such as Bose-Einstein condensation [43–45], supefluidity [46–48], and topological states of light [49]. Polariton interactions have potential applications in novel optical nonlinearities [50], polaritonic logical devices [51, 52], and quantum computing [35, 53, 54].

The Hamiltonian that describes the low-lying spectrum of the considered exciton-polariton condensate is given by

$$\hat{H} = -\Delta \hat{a}^\dagger \hat{a} + K \hat{a}^{\dagger 2} \hat{a}^2 - P_0(\hat{a} + \hat{a}^\dagger), \tag{2}$$

where $\hbar = 1$, $\hat{a}^\dagger$ ($\hat{a}$) is the creation (annihilation) operator, Δ is the pump-polariton detuning between the optical field frequency ϵ_0 and the lower-polariton mode $\epsilon_{\rm LP}$, $K = g\mathcal{C}_{\mathbf{0}}^4$ is the Kerr-like nonlinear interaction strength, with g being the bare exciton-exciton contact interaction and $\mathcal{C}_{\mathbf{0}}$ the Hopfield coefficient at zero momentum [39, 40], and P_0 is the effective optical pump, that depends on the quasi-mode coupling of the external field to the microcavity [55, 56] and the Hopfield coefficients. The three parameters in Eq. (2) are independently tunable in microcavity semiconductors via the light-matter detuning that modulates the polariton light-matter content. An illustration of the system is given in Fig. 1(a).

The exciton-polariton model in Eq. 2 does not exhibit a QPT. The energy gap between the ground-state energy and the first-excited energy does not close as we vary the parameters Δ, K or P_0; the ground state does not present any singularity. Yet, as we show below, the system presents an ESQPT, which affects the system's sensitivity all the way down to the ground state.

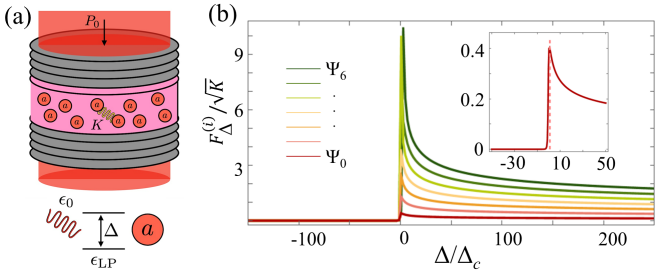

FIG. 1. (a) Illustration of the experimental setup: a microcavity semiconductor is pumped by an external coherent field with frequency ϵ_0 and effective amplitude P_0, creating a condensate of interacting exciton-polaritons with energy $\epsilon_{\rm LP}$. The exciton-polaritons are depicted as red spheres and their interaction strength is K. (b) Colored lines are the quantum Fisher information (QFI) for the first seven eigenstates as a function of the control parameter Δ; $P_0/K = 3$. The red line in the inset corresponds to the QFI of the ground state $|\Psi_0\rangle$ only and the dashed pink vertical line depicts the critical point of the ESQPT.

Quantum Fisher information divergence.— We set P_0/K constant and study the QFI as a function of the control parameter Δ in Fig. 1(b). According to the Hamiltonian in Eq. (2), the numerator in the equation for the QFI [Eq. (1)] involves the off-diagonal elements of the number operator, $\langle \Psi_i|\hat{n}|\Psi_j\rangle$, since $\partial_\Delta \hat{H} = -\hat{a}^\dagger \hat{a} = -\hat{n}$.

Figure 1(b) shows that $F_\Delta^{(j)}$ diverges when Δ reaches a value Δ_c. This is illustrated for the first seven lowest energy levels, including the ground state, which is also shown alone in the inset. This result indicates the enhanced sensitivity of the system at Δ_c. Our goal below is to provide the origin of this behavior.

Excited state quantum phase transition.— To understand the divergence of the QFI, we analyze the classical limit of Eq. (2), which is obtained using Glauber coherent states, $\hat{a}|\alpha\rangle = \alpha|\alpha\rangle$, where $\alpha = q + ip$. Expressed in terms of the canonical variables (q, p), the classical Hamiltonian reads

$$h_{cl} = \langle \alpha|\hat{H}|\alpha\rangle - \frac{\Delta}{2}(q^2+p^2) + \frac{K}{4}(q^2+p^2)^2 - \sqrt{2}P_0\, q, \tag{3}$$

where the classical energy is denoted by $h_{cl}(q,p) = \epsilon$. The roots of the Hamilton equations are

$$q_1 = -\frac{\beta}{\sqrt[3]{2}\,3^{2/3}K} - \frac{\sqrt[3]{\frac{2}{3}}\Delta}{\beta},$$
$$q_2 = \frac{\left(1+i\sqrt{3}\right)\Delta}{2^{2/3}\sqrt[3]{3}\beta} - \frac{\left(1-i\sqrt{3}\right)\beta}{2\sqrt[3]{2}\,3^{2/3}K},$$
$$q_3 = \frac{\left(1-i\sqrt{3}\right)\Delta}{2^{2/3}\sqrt[3]{3}\beta} + \frac{\left(1+i\sqrt{3}\right)\beta}{2\sqrt[3]{2}\,3^{2/3}K},$$

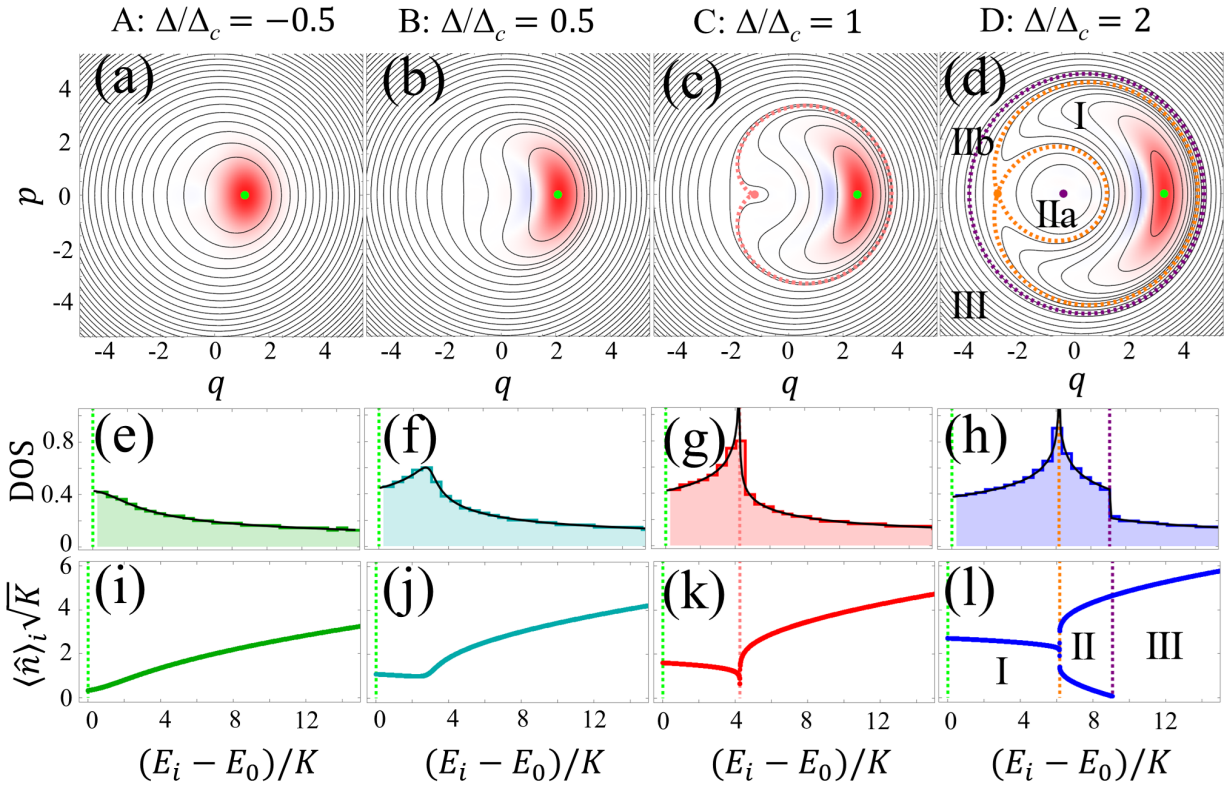

FIG. 2. (a)-(d) Phase space, where the green circle is the global minimum, the orange circle in (c)-(d) is the hyperbolic point, and the purple point in (d) is the local maximum. The black lines indicate the classical energy shells, the orange dotted line in (c)-(d) marks the energy $\epsilon_{\rm hyp}$ of the hyperbolic point, and the purple dotted line in (d) is the energy $\epsilon_{\rm max}$ associated with the local maximum. The red and blue shades indicate the positive and negative values of the Wigner function of the ground state $|\Psi_0\rangle$; $P_0/K = 3$. (e)-(h) Density of states (shaded area) and its classical limit (black line) for the same values of Δ/Δ_c. The vertical dotted orange (purple) line marks $\epsilon_{\rm hyp}$ ($\epsilon_{\rm max}$). (i)-(l) Expectation value of the number operator, $\langle\hat{n}\rangle_i$, as a function of the energies. The vertical dotted orange (purple) line marks $\epsilon_{\rm hyp}$ ($\epsilon_{\rm max}$). The roman numbers in (d) and (l) mark different regions of the phase space. In (e)-(l): $P_0/K = 1000$.

where $\beta = \sqrt[3]{\sqrt{6}\sqrt{27K^4P_0^2 + 2\Delta^3K^3} - 9\sqrt{2}K^2P_0}$. This implies that the classical system can have three critical points ($q = q_k, p = 0$) with $k = \{\min, \text{hyp}, \max\}$ indicating a global minimum (min), a hyperbolic point (hyp) and a global maximum (max). The global minimum is always present, being given by $q_{\rm min} = q_1$ when $\Delta < 0$ and $q_{\rm min} = q_2$ when $\Delta \geq 0$. The appearance of the other two points is determined by the critical point $\Delta_c = 3\sqrt[3]{KP_0^2/2}$. The hyperbolic point $q_{\rm hyp} = q_1$ appears when $\Delta \geq \Delta_c$ and the global maximum $q_{\rm max} = q_3$ when $\Delta > \Delta_c$. We denote the classical energies associated with the hyperbolic and local maximum points as $\epsilon_{\rm hyp}$ and $\epsilon_{\rm max}$, respectively.

The three critical points are shown in the phase spaces in Figs. 2(a)-(d), where the green circle is the global minimum, the orange circle appearing in Figs. 2(c)-(d) is the hyperbolic point, and the purple circle visible only in Fig. 2(d) is the global maximum. The black lines are the classical energy shells. The dotted orange line that intersects at the hyperbolic point (homoclinic orbit) in Fig. 2(c) marks the critical energy $\epsilon_{\rm hyp}$ of the separatrix that divides the phase space into two distinct regions. This line and the purple dotted line at $\epsilon_{\rm max}$ in Fig. 2(d) separate four regions of the phase space according to the energies: the region (I) of lowest energies ($\epsilon < \epsilon_{\rm hyp}$), the regions (IIa) and (IIb) of intermediate energies ($\epsilon_{\rm hyp} < \epsilon < \epsilon_{\rm max}$), and the outer region (III) of highest energies ($\epsilon > \epsilon_{\rm max}$).

The appearance of the hyperbolic point gets manifested in the quantum system and is responsible for the divergence of the QFI at $\Delta/\Delta_c = 1$ in Fig. 1(b). The hyperbolic point affects the spectrum and the structure of the eigenstates. In Figs. 2(e)-(h), we show the density of states (shaded area) and its classical limit (black line) obtained with the Gutzwiller trace formula [57]. The density of states diverges logarithmically in Figs. 2(g)-(h), where $\Delta \geq \Delta_c$. The divergence happens at the critical energy $E_{\rm ESQPT} \sim \epsilon_{\rm hyp}$ and is the principal signature of an ESQPT [27]. Our result shows that the ESQPT is dissociated from a QPT, which is absent for this system. There is also a step discontinuity in Fig. 2(h) at $E_{\rm step} \sim \epsilon_{\rm max}$, which reflects the presence of the local

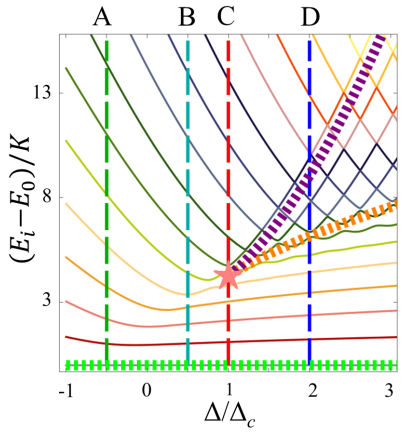

FIG. 3. Energy spectrum as function of Δ/Δ_c; $P_0/K = 3$. Dashed vertical lines indicate the spectrum at A ($\Delta/\Delta_c = -0.5$), B ($\Delta/\Delta_c = 0.5$), C ($\Delta/\Delta_c = 1$) and D ($\Delta/\Delta_c = 2$) analyzed in Fig. 2. The orange (purple) dashed line is the classical critical energy $\epsilon_{\rm hyp}$ ($\epsilon_{\rm max}$).

maximum.

The clustering of the energy levels that results in the divergence of the density of states in Figs. 2(e)-(h) can be verified in Fig. 3, where we show the eigenvalues E_i of the Hamiltonian in Eq. (2), subtracted from the ground-state energy E_0, as a function of the control parameter Δ. The orange star at $\Delta/\Delta_c = 1$ indicates the energy of the ESQPT, $E_{\rm ESQPT}$. This energy follows the dashed orange line for $\Delta > \Delta_c$. The clustering of the eigenvalues happens along this line. The figure also shows with a dashed purple line the energy $E_{\rm step} \sim \epsilon_{\rm max}$ of the step discontinuity seen in Fig. 2(h).

Between $E_{\rm ESQPT}$ and $E_{\rm step}$, the energy levels in Fig. 3 exhibit avoided crossings. This is associated with pairs of classical orbits, one orbit in region IIa and the other in region IIb of the phase space, as shown in Fig. 2(d), where the classical energies are equal. The values of Δ where the crossings occur can be obtained in the semiclassical limit using the Einstein-Brillouin-Keller quantization rule [58].

Eigenstate Structure.— The vertical lines in Fig. 3 indicate the selected values of Δ/Δ_c used to show the phase space in Figs. 2(a)-(d), the density of states in Figs. 2(e)-(h), as well as the expectation value of the number operator, $\langle\hat{n}\rangle_i$, as a function of the eigenvalue E_i in Figs. 2(i)-(l). These four last panels display the effects of the ESQPT on the structure of the eigenstates. A singularity appears at $E_{\rm ESQPT}$ in Figs. 2(k)-(l). The low value of $\langle\hat{n}\rangle_i$ at this point reflects the strong localization of the eigenstate at the ESQPT.

The expectation value of the number operator, $\langle\hat{n}\rangle_i$, coincides with the slope of an individual energy level $E_i(\Delta)$ according to the Hellmann–Feynman formula,

$$\frac{dE_i(\Delta)}{d\Delta} = \langle\Psi_i(\Delta)|\partial_\Delta \hat{H}|\Psi_i(\Delta)\rangle = \langle\hat{n}\rangle_i. \qquad (4)$$

These slopes appear explicitly in the equation for the level flow in the continuity equation [28],

$$j(\Delta, E) = \sum_i \frac{dE_i(\Delta)}{d\Delta}\delta(E - E_i(\Delta)), \qquad (5)$$

which identifies the ESQPT [59, 60]. This transition results in a dramatic modification of the energy landscape that gives rise to topological changes even in the vicinity of the ground state. These changes are detected by the QFI.

To show the effects of the ESQPT on the ground state, we depict with red (blue) shades in Figs. 2(a)-(d) the positive (negative) values of the Wigner function of the ground state. As Δ increases and approaches the ESQPT critical point, the ground state gets squeezed in q. The squeezing starts before the critical point, as in Fig. 2(b), and anticipates the appearance of the hyperbolic point. This behavior reflects the topology change created by the hyperbolic point and its homoclinic orbit. In fact, the squeezing of the ground state as the control parameter approaches the ESQPT critical point can be seen as an indirect signature of the ESQPT.

Conclusion.— Our study shows that a system of exciton-polaritons can be remotely taken into an ESQPT critical point through simple light frequency amplitude control. The clustering of the eigenvalues and the change in the structure of the eigenstates at the ESQPT combine to enhance the QFI, indicating an amplified sensitivity of the system. Our approach paves the way for the development of exponentially sensitive and remotely tunable sensing platforms.

Acknowledgements.— The authors acknowledge support from the National Science Foundation Engines Development Award: Advancing Quantum Technologies (CT) under Award Number 2302908. VSB also acknowledges partial support from the National Science Foundation Center for Quantum Dynamics on Modular Quantum Devices (CQD-MQD) under Award Number 2124511.

[1] C. L. Degen, F. Reinhard, and P. Cappellaro, Quantum sensing, Rev. Mod. Phys. **89**, 035002 (2017).
[2] D. Braun, G. Adesso, F. Benatti, R. Floreanini, U. Marzolino, M. W. Mitchell, and S. Pirandola, Quantum-enhanced measurements without entanglement, Rev. Mod. Phys. **90**, 035006 (2018).
[3] G. M. D'Ariano, P. Lo Presti, and M. G. A. Paris, Using Entanglement Improves the Precision of Quantum Measurements, Phys. Rev. Lett. **87**, 270404 (2001).
[4] A. Acín, Statistical Distinguishability between Unitary Operations, Phys. Rev. Lett. **87**, 177901 (2001).
[5] V. Giovannetti, S. Lloyd, and L. Maccone, Quantum-enhanced positioning and clock synchronization, Nature **412**, 417 (2001).

[6] V. Giovannetti, S. Lloyd, and L. Maccone, Quantum-enhanced measurements: Beating the standard quantum limit, Science **306**, 1330 (2004).

[7] V. Giovannetti, S. Lloyd, and L. Maccone, Quantum Metrology, Phys. Rev. Lett. **96**, 010401 (2006).

[8] C. M. Caves, Quantum-mechanical noise in an interferometer, Phys. Rev. D **23**, 1693 (1981).

[9] J. Abadie *et al.*, A gravitational wave observatory operating beyond the quantum shot-noise limit, Nat. Phys. **7**, 962 (2011).

[10] P. Zanardi, M. G. A. Paris, and L. Campos Venuti, Quantum criticality as a resource for quantum estimation, Phys. Rev. A **78**, 042105 (2008).

[11] M. Tsang, Quantum transition-edge detectors, Phys. Rev. A **88**, 021801 (2013).

[12] S. Fernández-Lorenzo and D. Porras, Quantum sensing close to a dissipative phase transition: Symmetry breaking and criticality as metrological resources, Phys. Rev. A **96**, 013817 (2017).

[13] M. M. Rams, P. Sierant, O. Dutta, P. Horodecki, and J. Zakrzewski, At the Limits of Criticality-Based Quantum Metrology: Apparent Super-Heisenberg Scaling Revisited, Phys. Rev. X **8**, 021022 (2018).

[14] L. Garbe, M. Bina, A. Keller, M. G. A. Paris, and S. Felicetti, Critical Quantum Metrology with a Finite-Component Quantum Phase Transition, Phys. Rev. Lett. **124**, 120504 (2020).

[15] K. Gietka, F. Metz, T. Keller, and J. Li, Adiabatic critical quantum metrology cannot reach the Heisenberg limit even when shortcuts to adiabaticity are applied, Quantum **5**, 489 (2021).

[16] Y. Chu, S. Zhang, B. Yu, and J. Cai, Dynamic Framework for Criticality-Enhanced Quantum Sensing, Phys. Rev. Lett. **126**, 010502 (2021).

[17] M. Salado-Mejía, R. Román-Ancheyta, F. Soto-Eguibar, and H. M. Moya-Cessa, Spectroscopy and critical quantum thermometry in the ultrastrong coupling regime, Quantum Sci. Technol. **6**, 025010 (2021).

[18] T. Ilias, D. Yang, S. F. Huelga, and M. B. Plenio, Criticality-Enhanced Quantum Sensing via Continuous Measurement, PRX Quantum **3**, 010354 (2022).

[19] L. Garbe, O. Abah, S. Felicetti, and R. Puebla, Critical quantum metrology with fully-connected models: from Heisenberg to Kibble–Zurek scaling, Quantum Sci. Technol. **7**, 035010 (2022).

[20] D.-S. Ding, Z.-K. Liu, B.-S. Shi, G.-C. Guo, K. Mølmer, and C. S. Adams, Enhanced metrology at the critical point of a many-body Rydberg atomic system, Nat. Phys. **18**, 1447 (2022).

[21] R. Di Candia, F. Minganti, K. V. Petrovnin, G. S. Paraoanu, and S. Felicetti, Critical parametric quantum sensing, npj Quantum Inf. **9**, 23 (2023).

[22] C. Hotter, H. Ritsch, and K. Gietka, Combining Critical and Quantum Metrology, Phys. Rev. Lett. **132**, 060801 (2024).

[23] S. L. Braunstein and C. M. Caves, Statistical distance and the geometry of quantum states, Phys. Rev. Lett. **72**, 3439 (1994).

[24] S. L. Braunstein, C. M. Caves, and G. Milburn, Generalized uncertainty relations: Theory, examples, and lorentz invariance, Ann. Phys. **247**, 135 (1996).

[25] W.-L. You, Y.-W. Li, and S.-J. Gu, Fidelity, dynamic structure factor, and susceptibility in critical phenomena, Phys. Rev. E **76**, 022101 (2007).

[26] L. Campos Venuti and P. Zanardi, Quantum Critical Scaling of the Geometric Tensors, Phys. Rev. Lett. **99**, 095701 (2007).

[27] M. Caprio, P. Cejnar, and F. Iachello, Excited state quantum phase transitions in many-body systems, Ann. of Phys. **323**, 1106 (2008).

[28] P. Cejnar, P. Stránský, M. Macek, and M. Kloc, Excited-state quantum phase transitions, J. Phys. A **54**, 133001 (2021).

[29] L. F. Santos and F. Pérez-Bernal, Structure of eigenstates and quench dynamics at an excited-state quantum phase transition, Phys. Rev. A **92**, 050101 (2015).

[30] L. F. Santos, M. Távora, and F. Pérez-Bernal, Excited-state quantum phase transitions in many-body systems with infinite-range interaction: Localization, dynamics, and bifurcation, Phys. Rev. A **94**, 012113 (2016).

[31] L. Garbe, O. Abah, S. Felicetti, and R. Puebla, Exponential time-scaling of estimation precision by reaching a quantum critical point, Phys. Rev. Res. **4**, 043061 (2022).

[32] T. L. Heugel, M. Biondi, O. Zilberberg, and R. Chitra, Quantum Transducer Using a Parametric Driven-Dissipative Phase Transition, Phys. Rev. Lett. **123**, 173601 (2019).

[33] N. E. Frattini, R. G. Cortiñas, J. Venkatraman, X. Xiao, Q. Su, C. U. Lei, B. J. Chapman, V. R. Joshi, S. M. Girvin, R. J. Schoelkopf, S. Puri, and M. H. Devoret, The squeezed Kerr oscillator: spectral kissing and phase-flip robustness (2022), arXiv:2209.03934.

[34] J. Chávez-Carlos, T. L. M. Lezama, R. G. Cortiñas, J. Venkatraman, M. H. Devoret, V. S. Batista, F. Pérez-Bernal, and L. F. Santos, Spectral kissing and its dynamical consequences in the squeeze-driven Kerr oscillator, npj Quantum Inf. **9**, 10.1038/s41534-023-00745-1 (2023).

[35] S. Ghosh and T. C. H. Liew, Quantum computing with exciton-polariton condensates, npj Quantum Inf. **6**, 16 (2020).

[36] C. Ciuti and I. Carusotto, Quantum fluid effects and parametric instabilities in microcavities, Phys. Status Solidi (b) **242**, 2224 (2005).

[37] A. Amo and J. Bloch, Exciton-polaritons in lattices: A non-linear photonic simulator, C. R. Phys. **17**, 934 (2016).

[38] T. Byrnes, N. Y. Kim, and Y. Yamamoto, Exciton–polariton condensates, Nature Physics **10**, 803 (2014).

[39] I. Carusotto and C. Ciuti, Quantum fluids of light, Rev. Mod. Phys. **85**, 299 (2013).

[40] J. Hopfield, Theory of the contribution of excitons to the complex dielectric constant of crystals, Phys. Rev. **112**, 1555 (1958).

[41] B. Deveaud, Polariton interactions in semiconductor microcavities, C. R. Phys. **17**, 874 (2016).

[42] J. Bloch, I. Carusotto, and M. Wouters, Non-equilibrium bose-einstein condensation in photonic systems, Nat. Rev. Phys. **4**, 470 (2022).

[43] A. Amo, D. Sanvitto, F. Laussy, D. Ballarini, E. d. Valle, M. Martin, A. Lemaitre, J. Bloch, D. Krizhanovskii, M. Skolnick, *et al.*, Collective fluid dynamics of a polariton condensate in a semiconductor microcavity, Nature **457**, 291 (2009).

[44] J. Kasprzak, M. Richard, S. Kundermann, A. Baas, P. Jeambrun, J. M. J. Keeling, F. Marchetti, M. Szymańska, R. André, J. Staehli, *et al.*, Bose–einstein condensation of exciton polaritons, Nature **443**, 409 (2006).

[45] H. Deng, H. Haug, and Y. Yamamoto, Exciton-polariton bose-einstein condensation, Rev. Mod. Phys. **82**, 1489 (2010).
[46] A. Amo, J. Lefrère, S. Pigeon, C. Adrados, C. Ciuti, I. Carusotto, R. Houdré, E. Giacobino, and A. Bramati, Superfluidity of polaritons in semiconductor microcavities, Nat. Phys. **5**, 805 (2009).
[47] D. Sanvitto, S. Pigeon, A. Amo, D. Ballarini, M. De Giorgi, I. Carusotto, R. Hivet, F. Pisanello, V. G. Sala, P. S. S. Guimaraes, R. Houdré, E. Giacobino, C. Ciuti, A. Bramati, and G. Gigli, All-optical control of the quantum flow of a polariton condensate, Nat. Photonics **5**, 610 (2011).
[48] G. Lerario, A. Fieramosca, F. Barachati, D. Ballarini, K. S. Daskalakis, L. Dominici, M. De Giorgi, S. A. Maier, G. Gigli, S. Kéna-Cohen, and D. Sanvitto, Room-temperature superfluidity in a polariton condensate, Nat. Phys. **13**, 837 (2017).
[49] T. Ozawa, H. M. Price, A. Amo, N. Goldman, M. Hafezi, L. Lu, M. C. Rechtsman, D. Schuster, J. Simon, O. Zilberberg, and I. Carusotto, Topological photonics, Rev. Mod. Phys. **91**, 015006 (2019).
[50] D. N. Basov, A. Asenjo-Garcia, P. J. Schuck, X. Zhu, and A. Rubio, Nanophotonics **10**, 549 (2021).
[51] D. Ballarini, M. De Giorgi, E. Cancellieri, R. Houdré, E. Giacobino, R. Cingolani, A. Bramati, G. Gigli, and D. Sanvitto, All-optical polariton transistor, Nat. Commun. **4**, 1778 (2013).
[52] D. Sanvitto and S. Kéna-Cohen, The road towards polaritonic devices, Nat. Mater. **15**, 1061 (2016).
[53] Y. Xue, I. Chestnov, E. Sedov, E. Kiktenko, A. K. Fedorov, S. Schumacher, X. Ma, and A. Kavokin, Split-ring polariton condensates as macroscopic two-level quantum systems, Phys. Rev. Res. **3**, 013099 (2021).
[54] A. Kavokin, T. C. H. Liew, C. Schneider, P. G. Lagoudakis, S. Klembt, and S. Hoefling, Polariton condensates for classical and quantum computing, Nature Reviews Physics **4**, 435 (2022).
[55] N. Takemura, S. Trebaol, M. Wouters, M. T. Portella-Oberli, and B. Deveaud, Polaritonic feshbach resonance, Nat. Phys. **10**, 500 (2014).
[56] C. Ciuti, P. Schwendimann, and A. Quattropani, Theory of polariton parametric interactions in semiconductor microcavities, Semicond. Sci. Technol. **18**, S279 (2003).
[57] M. C. Gutzwiller, *Chaos in Classical and Quantum Mechanics* (Springer, New York, 1990).
[58] M. A. P. Reynoso, D. J. Nader, J. Chávez-Carlos, B. E. Ordaz-Mendoza, R. G. Cortiñas, V. S. Batista, S. Lerma-Hernández, F. Pérez-Bernal, and L. F. Santos, Quantum tunneling and level crossings in the squeeze-driven kerr oscillator, Phys. Rev. A **108**, 033709 (2023).
[59] P. Stransky, M. Macek, and P. Cejnar, Excited-state quantum phase transitions in systems with two degrees of freedom: Level density, level dynamics, thermal properties, Ann. Phys. **345**, 73 (2014).
[60] P. Stránský and P. Cejnar, Classification of excited-state quantum phase transitions for arbitrary number of degrees of freedom, Phys. Lett. A **380**, 2637–2643 (2016).